Supplementary information

S1 Photovoltaic cell design and fabrication:

We use a thin-film $In_{0.55}Ga_{0.45}As$ photovoltaic cell with a bandgap of 0.75eV (Fig. 5). InGaAs, like all III-V semiconductors, can have an excellent radiative recombination coefficient[1]. The device is a heterojunction structure where the active material is sandwiched between a hole selective p-InP layer, and an electron selective n-InP layer. These two heterojunction layers are Ohmically contacted by thin, heavily-doped, front n-InGaAs and rear p-InGaAsP layers, which are covered by thin-film Au electrodes. The Au electrodes are then connected to the external circuit using aluminum wire-bonds. We note that while the front electrode grid might induce shadowing losses in a typical photovoltaic system, in our thermophotovoltaic system those photons are reflected back into the emitter and recovered. Indeed, the reflectivity of the Au/Air interface is 98%, and therefore parasitic absorption by the front electrode is negligible. Moreover, the InGaAsP and InP heterojunction layers in the device have higher bandgap (1eV and 1.34eV respectively) than the active layer (0.75eV), to ensure that parasitic absorption within these layers are also minimized. The architecture of these cells is a "rear heterojunction" (RHJ) with the p-n junction at the heterojunction between the n-type InGaAs absorber and a higher bandgap p-type InP confinement layer. The heterojunction lowers the recombination current, effectively increasing the voltage. The significantly higher mobility of the electrons in n-type material, compared to holes in p-type material, also leads to lower free carrier absorption. In addition the higher electron mobility assists the sheet conductivity.

These layers are grown by atmospheric pressure metalorganic vapor phase epitaxy on an InP substrate. The growth is inverted, with top layer grown first, and the device is re-oriented during

post-growth processing. After the deposition of the gold film—which is used both as the mirror and the positive electrode—the layer stacks are then attached to a silicon handle using a thermally conductive epoxy. The InP substrate is then totally etched away.

S2 Chamber design for thermophotovoltaics:

The photovoltaic cell is placed under a copper baffle that provides an aperture for defining the incident radiation pattern (Fig. 4). The copper baffle was heat sunk to the base of the chamber, which was kept at ~20°C throughout the duration of the experiment. The temperature at the top of the baffle reached at most 70°C. At~1207°C, the total power flux from the emitter is 300 times stronger than the power flux from the baffle. Thus, the overall effect is negligible compared to the effect of reflectivity measurement uncertainty, as we describe in the error analysis section.

The inner walls of the baffle are coated with a highly absorptive black coating, to eliminate stray photons between the baffle and the photovoltaic cell. This replicates the situation in a thermophotovoltaic system with an emitter fully surrounded by photovoltaic cells, where these stray reflected photons would be re-captured by the heat source. The entire system is placed inside a vacuum chamber with a pressure of 10^{-5} Torr. The vacuum minimizes any parasitic heat conduction from the emitter to the photovoltaic cell.

S3 Graphite emissivity measurement

The emitter, a thin graphite strip, is held in place by copper mounts on either side, as shown in Fig. S1. Electrical power is injected to the graphite through the copper mount, resulting in Joule

heating of the graphite emitter. At a steady emitter temperature T_s, electrical power injected to the graphite and copper mount system is converted to heat in two ways: radiation through graphite (due to high emissivity ε of the graphite) and Joule heating via the contact resistance (R_c) in the copper mount,

$$P_{\text{injected}}(T_s) = V_{\text{AC}}(T_s)I_{\text{AC}}(T_s) = I_{\text{AC}}^2(T_s)R_{\text{C}} + A_{\text{emitter}}\varepsilon \int_0^\infty b_s(E,T_s)\cdot EdE, \quad \text{(S1)}$$

where $V_{AC}(T_s)$, $I_{AC}(T_s)$ are the RMS voltage and current injected into the mount-emitter system for an emitter temperature T_s and $A_{emitter}$ is the surface area of the emitter (98mm. ×14mm.). At a given emitter temperature T_s with known values of the $V_{AC}(T_s)$ and $I_{AC}(T_s)$, the only unknowns in Eq'n (S1) are the contact resistance R_c and emissivity ε. Hence, we can construct a system of equations with two closely spaced emitter temperatures (to reduce the effect from the temperature dependence of R_c) using Eq'n (S1), and then solve for both R_c and ε. We measure an emissivity ε= 0.91 for graphite, consistent with reported values from Neuer[2].

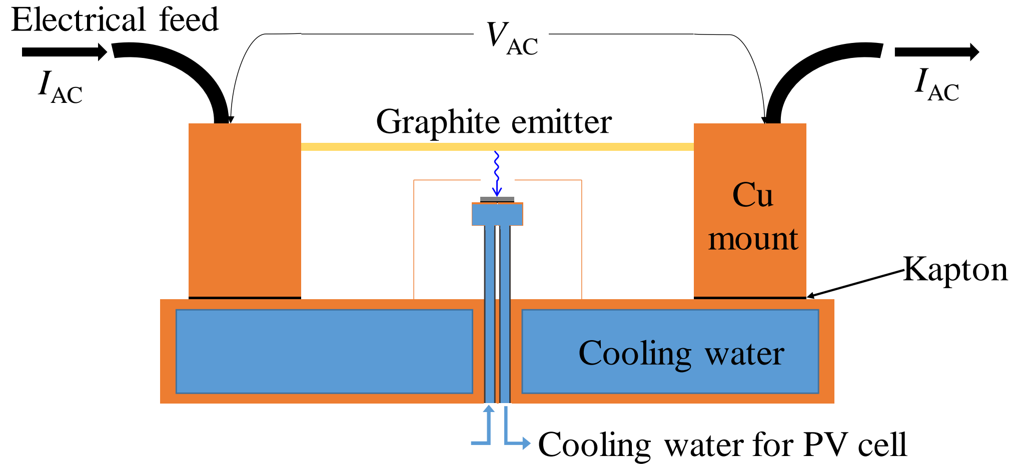

Figure S1: Cross-section of the setup. Graphite is heated by Joule heating. The supplies electrical power to the mount and emitter system can be converted to heat in two ways, either emission through graphite or resistive heating of the mount itself, as well as the contact resistance of the of the mount and emitter.

S4 Measurement of reflectivity and external quantum efficiency:

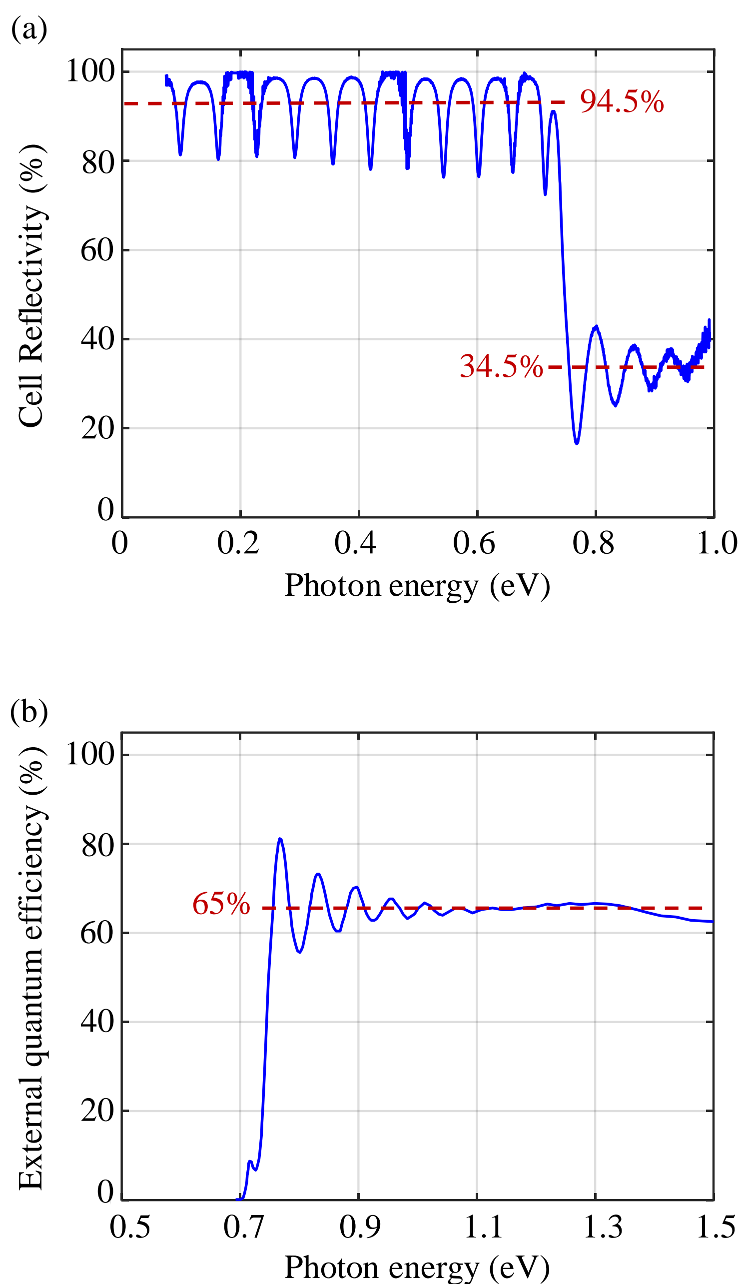

Figure S2: (a) Reflectivity spectrum of one of the photovoltaic cell used in our experiment. The average below-bandgap reflectivity is 94.5%. The average reflectivity is 34.5% in the semiconductor absorbing region. The periodic dips result from thin-film interference among the device layers. (b) External quantum efficiency of the same photovoltaic cell.

We measure the reflectivity of our cells using a Fourier transform infrared (FTIR) spectrometer. The result from a representative device, with a reflectivity almost the same as batch average, is shown in Fig. S2(a)). The incident and reflected light pass through a microscope objective with a numerical aperture (NA)=0.65, which corresponds to an angular reflectivity averaged over an incidence angle range, of 0° to 36° from normal. The reflectivity oscillations in Fig. S2(a) result from the expected thin-film interference in the semiconductor film. The average reflectivity for our devices, weighted by the Planck spectrum of thermal emission at 1200°C, for energies below the band edge, is 94.6%, corrected for the 0.5% systematic error in our FTIR setup. This is lower than the 98% reflectivity of air-gold interface, due to the higher refractive index n=3.5 in the semiconductor, which reduces the critical angle at the semiconductor-gold interface. The measured reflectivity is 34.5% for energies above the band edge, primarily due to Fresnel reflection at the air-semiconductor interface. These reflected photons undergo thermal regeneration in the emitter

The external quantum efficiency of the cell, shown in Fig. S2(b), is the fraction of photons incident on the front surface that are converted to electron-hole pairs and collected at the device terminals. The deviation of this value from 100% for energies above the bandgap is primarily due to the lack of an anti-reflection coating on the photovoltaic cell.

S5 Error analysis*:*

The thermophotovoltaic power efficiency is the ratio of $P_{\text{electrical}}$, the electrical power generated by the cell, to P_{absorbed}, the power absorbed by the cell. Since $P_{\text{electrical}}$ is measured with a high-precision sourcemeter, the error in the efficiency is dominated by P_{absorbed}. Hence, according to Eq'n. (5), the error arises from uncertainties in the measurement of graphite emissivity (ε), the cell absorptivity (1-R), and the emitter temperature, the last of which leads to an error in the Planck

radiance (b_s). However, any uncertainty in emissivity is cancelled by an equal and opposite change in the value of view factor F_{eff}, from Eq'n. (4)-(5). Hence the TPV efficiency uncertainty can be expressed through RMS addition as:

$$\frac{\triangle\eta}{\eta} = \sqrt{\left(\frac{\triangle a}{a}\right)^2 + \left(\frac{\triangle b_s}{b_s}\right)^2} \tag{S2}$$

The absolute uncertainty in absorptivity $\triangle a$ ($\equiv\triangle R$) is 0.2%, due to statistical error in the measurement. The average absorptivity a is weighted by the incident Planck power spectrum at every temperature. For T_s = 1207°C, the average absorptivity is 14.5%, including above and below bandgap, resulting in a relative error $\left(\frac{\triangle a}{a}\right)$= 0.014 for absorptivity.

The Planck spectrum at any given emitter temperature is determined from the measurement of the short-circuit current, as shown in Eq'n. (4). Since the current can be measured very accurately, the uncertainty in measuring b_s is dependent on the uncertainty of the EQE measurement:

$$\frac{\triangle b_s}{b_s} = \frac{\triangle \mathrm{EQE}}{\mathrm{EQE}} \tag{S3}$$

A brute force calculation for the photovoltaic cell indicate an EQE in the range 65±1.95%, but a more focused analysis based on V_{oc} indicates that 65±1.3% would be more appropriate. Thus the △EQE/EQE will be completely dominated by the error in absorptivity, by order of magnitude. Thus the error will be primarily contributed by the error in absorptivity measurement. Hence, from Eq'n. (S2), we find a relative uncertainty $\frac{\triangle\eta}{\eta}$ =1.4% in our measured thermophotovoltaic efficiency, resulting an absolute error of 29.1×.014=0.4%.

S6 Electrical measurements

In Fig. S3 we show the data corresponding to illumination under different emitter temperatures, for the representative device. The dark curves are shown in Fig. S4. The open circuit voltage (V_{oc}),

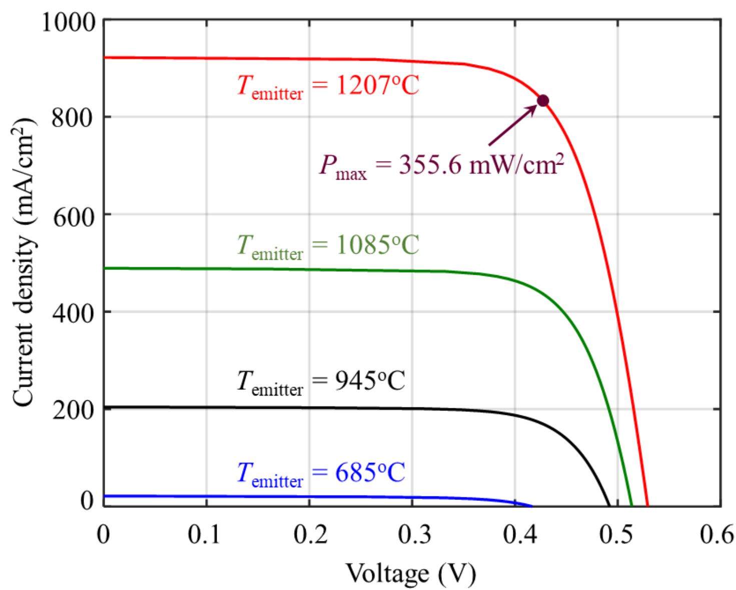

Figure S3: Current-voltage curves for the InGaAs cell at different emitter temperatures.

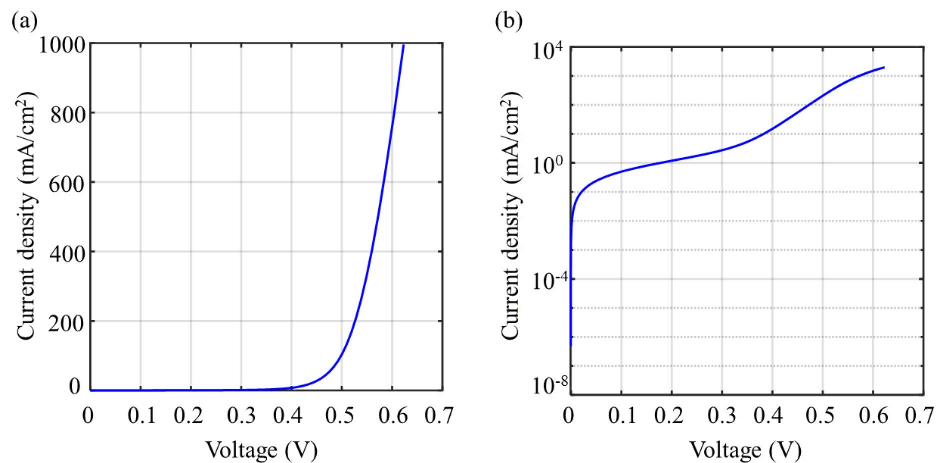

Figure S4: Measured dark currrent of a photovoltaic device. (a) shows the data in linear scale, (b) in semilog scale. From the slope of the curve, R_s is found to be ~0.43Ω. A high shunt conductance is visible in (b), at low bias (<0.35V). We calculated the shunt resistance to be ~854Ω.

Table S1: Experimental data on current-voltage properties of the photovoltaic cell at different emitter temperatures. The current density, J_{SC} is calculated by dividing the current the cell area, 10.04mm^2.

emitter temperature (Celsius)	J_{SC} (mA/cm^2)	V_{OC} (mV)	Fill Factor (%)
685	22.71	418.98	65.39
764	49.30	449.86	71.71
836	91.63	468.03	73.18
891	140.44	481.23	73.55
945	204.98	492.13	74.30
990	277.29	500.91	74.89
1039	372.91	507.66	74.51
1085	487.65	513.78	74.76
1131	624.70	518.98	74.36
1177	790.64	523.35	73.44
1207	917.83	529.20	73.37

short-circuit current (J_{sc}) and fill-factor of the device under illumination are also given in the accompanying table S1.

S7 Device modelling

The current density J in the photovoltaic cell can be described as $J(T_s,V) = J_L(T_s) - J_{diode}(V)$, where J_L is photo-generated current density and J_{diode} is the current arising from carrier removal, as a consequence of the bias applied to the diode. This diode current has three main components; (a) carriers that recombine radiatively and produce photons that escape out of the device (J_{esc}), (b) carriers that produce photons that are lost by parasitic absorption in the mirror (J_{mirror}) and, (3)

carriers that are lost due to non-radiative SRH or Auger recombination within the device (J_{nrad}). Hence, we can write J as:

$$J(T_s,V) = J_L(T_s) - J_{esc}(V) - J_{mirror}(V) - J_{nr_{ad}}(V) \tag{S4}$$

We can calculate $J_L(T_s)$ for an arbitrary emitter temperature T_s from Eq'n. (S5), where $a(E)$ is the absorptivity spectrum and IQE(E) is the internal quantum efficiency—fraction of the generated carriers that is extracted by the electrical contacts—of the cell. For a cell with planar geometry, we can express $a(E)$ with Eq'n. (S6), where T_{front} is the transmissivity of the front surface, and $R_{rear}(E)$ is the reflectivity of the rear mirror. T_{front} was taken to be 65.5%, obtained from an above-bandgap spectral average of the measured reflectivity spectrum, and IQE was taken to be 98%, accounting for a small loss due to non-unity carrier collection efficiency. The absorption co-efficient $\alpha(E)$ is taken as the average of that of GaAs and InAs, weighted by material composition, similar to Ganapati et. al. [3].

$$J_L(T_s) = q\int_0^\infty a(E)b_s(T_s,E)\text{IQE}(E)\,dE \tag{S5}$$

$$a(E) = T_{front}\frac{(1-\exp(-\alpha(E)L))}{1-(1-T_{front})R_{rear}(E)\exp(-2\alpha(E)L)}(1+R_{rear}(E)\exp(-\alpha(E)L)) \tag{S6}$$

An internal luminescent current exists within the device (J_{rad}) under an applied bias. The portion of this internal current that escapes through the front, $J_{esc}(V)$can be expressed as $P_{esc}\cdot J_{rad}(V)$, where P_{esc} is the escape probability of a photon inside the device. We can express P_{esc} as in Eq'n. (S7), which has been derived by Rau et. al.[4]. The temperature of the cell is denoted by T_c. For this calculation, we used a refractive index n_r=3.5. We can calculate $J_{rad}(V)$ from the modified Shockley-Van-Roosebroeck relationship, as in Eq'n. (S8)[5].

$$P_{esc} = \frac{\int_0^\infty a(E)b_s(T_c,E)\,dE}{\int_0^\infty 4n_r^2L\alpha(E)b_s(T_c,E)dE} \tag{S7}$$

$$J_{\mathrm{rad}}(V) = qnp\frac{2\pi L}{c^2h^3}\int_0^{\infty} 4n_{\mathrm{r}}^2E^2\alpha(E)\exp\left(\frac{qV-E}{K_{\mathrm{b}}T_{\mathrm{c}}}\right)dE \tag{S8}$$

A portion of the radiative recombination current is lost by mirror absorption, rather than extracted through the front surface. The mirror loss can be expressed as $P_{\mathrm{mirror}}J_{\mathrm{rad}}(\mathrm{V})$, where P_{mirror} is the probability that an internally emitted photon is absorbed by the mirror. This probability is given by Eq'n. (S9), where $a_{\mathrm{rear}}(E,\Theta)$ is the absorptivity of the mirror for photons internally emitted inside the semiconductor. The expression for a_{rear} can be found by equating the rate of absorption of luminescent photons by the rear to the mirror's rate of thermal radiation. An expression for $a_{\mathrm{rear}}(E,\Theta)$ in a planar structure such as ours has been derived in Ganapati et. al. [3,6], and is given by Eq'n. (S10), where $\Theta_{\mathrm{c}} = \sin^{-1}(1/n_r)$ is the critical angle of the front air-semiconductor interface. In Eq'n. (S9), we have a factor of n_{r}^2 which is absent in Eq'n. (S6). This is due to the fact that the mirror radiates into the semiconductor, where the density of electromagnetic modes is greater by a factor of n_{r}^2 relative to air.

$$P_{\mathrm{mirror}} = \frac{\int_0^{\infty} n_{\mathrm{r}}^2 a_{\mathrm{rear}}(E,\Theta)(E)b_{\mathrm{s}}(E,T_{\mathrm{c}})dE}{\int_0^{\infty} 4n_{\mathrm{r}}^2 L\alpha(E)b_{\mathrm{s}}(E,T_{\mathrm{c}})dE} \tag{S9}$$

$$a_{\mathrm{rear}}(E,\Theta) = (1-R_{\mathrm{rear}})\times\begin{cases}1-\exp\left(-\frac{\alpha(E)L}{\cos\Theta}\right), & \text{if } \Theta<\Theta_c\\ \frac{1-\exp\left(-\frac{2\alpha(E)L}{\cos\Theta}\right)}{1-R(E)\exp\left(-\frac{2\alpha(E)L}{\cos\Theta}\right)}, & \text{if } \Theta\geq\Theta_c\end{cases} \tag{S10}$$

The remaining component $J_{\mathrm{nrad}}(V)$, can be estimated from the internal luminescence efficiency $\eta_{\mathrm{int}}(V)$, expressed as:

$$\eta_{\mathrm{int}}(V) = \frac{J_{\mathrm{rad}}(V)}{J_{\mathrm{rad}}(V)+J_{\mathrm{nrad}}(V)}. \tag{S11}$$

Re-arranging terms, we get

$$J_{\mathrm{nrad}}(V) = \left(\frac{1}{\eta_{\mathrm{int}}(V)}-1\right)J_{\mathrm{rad}}(V). \tag{S12}$$

Knowing the *J-V* under any illumination, we can then estimate the $\eta_{int}(V)$ using Eq'n. (S3)-(S11), and vice versa.

Finally, we include the effects of the series resistance R_s and the shunt resistance R_{sh} by using the modified current equation, Eq'n. (S13). We can account for the effect of series resistance by replacing the terminal voltage V in Eq'n. (S4)-(S12) with $V+J\cdot R_s\cdot A$, which is the quasi-Fermi level splitting inside the InGaAs layer. We can estimate the series resistance R_s from the slope of the measured I-V curve at open-circuit voltage, which gives $R_s= 0.43\Omega$. Fitting the measured dark *J-V* curve to Eq'n. (S13), this leads to an average $\eta_{int}= 82\%$ and shunt resistance $R_{sh}= 852\Omega$. We note that near the operating voltage of the cell, the effect of R_{sh} is minimal, and hence the deviation of our photovoltaic cell performance from ideal is determined by the values of R_s, $R(E)$ and $\eta_{int}(V)$.

$$J(T_s, V+JR_sA) = J_L(T_s) - J_{esc}(V+JR_sA) - J_{mirror}(V+JR_sA) - J_{nrad}(V+JR_sA) - \frac{V+JR_sA}{R_{sh}A} \tag{S13}$$

Knowing the value of $\eta_{int}(V)$ allows us to calculate the SRH lifetime, τ_{SRH} for this device, using Eq'n. (S13), where n and p are the electron and hole concentration and n_i as the intrinsic carrier density. We used the Auger coefficients C_n and C_p to be 8.1×10^{-29}cm^{6}s^{-1} from the experimental data of Ahrenkiel et. al.[7]. To calculate the carrier densities, we used the reported values of the electronic parameters of InGaAs[8].

$$J_{nrad} = L\left[\frac{np-n_i^2}{\tau_{SRH}(n+p+2n_i)} + (C_n n + C_p p)(np - n_i^2)\right] \tag{S14}$$

Fitting the measured value of η_{int} to this expression yields τ_{SRH}= 60 ns. With improved materials processing, there is potential to increase this lifetime by more than two orders of magnitude [7], which in turn would increase the value of η_{int}= 98%.

S8 Limit of Series Resistance

The series resistance of the device (prior to making wirebonds) was 0.1Ω. The grids contributed 0.09Ω (for 200µm spacing between gridlines, which are 5µm wide and 2µm thickness, and a total device area of 3.13×3.13 sq. mm. [9]) while the remaining 0.01Ω was due to contact and semiconductor sheet resistance. Improvement in the grid geometry (e.g. by increasing the width and thickness of the gridlines) can reduce the grid resistance below 0.1Ω, leaving only the contact and sheet resistance as the limiting series resistance of the device. Hence for the material stack of our device, 0.01Ω is the limit of series resistance.

S9 Effect of anti-reflection coating

The regenerative TPV system depends on the use of a highly reflective mirror. In the presence of a poor mirror, insufficiently strong absorptivity of high-energy photons might result in parasitic losses. Any photons that undergo Fresnel reflection will be absorbed and regenerated inside the

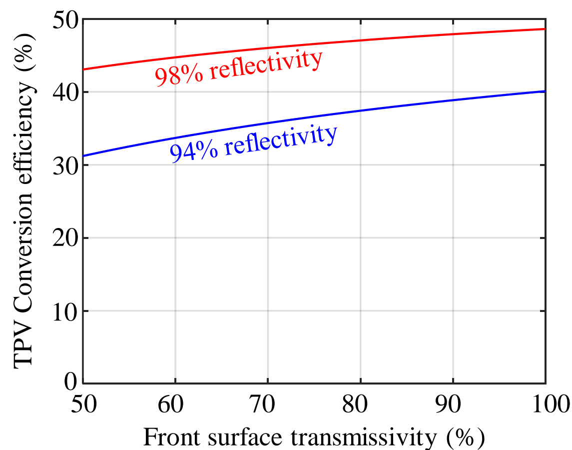

Figure S5: Effect of anti-reflection coating. In presence of a relatively poor mirror, anti-reflection coating increases device efficiency.

emitter. For a bandgap =0.75eV, photons reabsorbed by the mirror will have a higher probability of being regenerated as low-energy photons, for emitter temperatures <3000°C. These regenerated photons undergo a second chance of being lost due to parasitic absorption in the poor mirror. The addition of an anti-reflection coating can reduce this loss, as shown in Fig. (S5).

A better rear mirror reduces the loss of low-energy photons, hence the gain in thermophotovoltaic efficiency with anti-reflection coating is lower for photovoltaic cells with better mirror, than for cells with poor mirror. This is evident when the slopes of the two curves are compared in Fig. (S5).

---

[1] R. K. Ahrenkiel, R. Ellingson, S. Johnston, and M. Wanlass, "Recombination lifetime of In0.53Ga0.47As as a function of doping density," *Appl. Phys. Lett.*, vol. 72, no. 26, pp. 3470–3472, Jun. 1998.
[2] G. Neuer, "Spectral and total emissivity measurements of highly emitting materials," *Int. J. Thermophys.*, vol. 16, no. 1, pp. 257–265, Jan. 1995.
[3] V. Ganapati, T. Patrick Xiao, and E. Yablonovitch, "Ultra-efficient thermophotovoltaics exploiting spectral Filtering by the Photovoltaic Band-Edge," *ArXiv161103544 Phys.*, Nov. 2016.
[4] U. Rau, U. W. Paetzold, and T. Kirchartz, "Thermodynamics of light management in photovoltaic devices," *Phys. Rev. B*, vol. 90, no. 3, p. 035211, Jul. 2014.
[5] W. van Roosbroeck and W. Shockley, "Photon-Radiative Recombination of Electrons and Holes in Germanium," *Phys. Rev.*, vol. 94, no. 6, pp. 1558–1560, Jun. 1954.
[6] V. Ganapati, M. A. Steiner, and E. Yablonovitch, "The Voltage Boost Enabled by Luminescence Extraction in Solar Cells," *IEEE J. Photovolt.*, vol. 6, no. 4, pp. 801–809, Jul. 2016.
[7] R. K. Ahrenkiel, R. Ellingson, S. Johnston, and M. Wanlass, "Recombination lifetime of In0.53Ga0.47As as a function of doping density," *Appl. Phys. Lett.*, vol. 72, no. 26, pp. 3470–3472, Jun. 1998.
[8] "Recombination Parameter of Gallium Indium Arsenide (GaInAs)." [Online]. Available: http://www.ioffe.ru/SVA/NSM/Semicond/GaInAs/recombination.html#Recombination. [Accessed: 16-Apr-2018].
[9] "Finger Resistance | PVEducation." [Online]. Available: https://www.pveducation.org/pvcdrom/design/finger-resistance. [Accessed: 06-Jul-2018].